Letter

Triboelectric charge transfer theory driven by thermoelectric effect

Ji-Ho Mun [1,*] Eui-Cheol Shin [1,*] Jaeuk Seo [1] and Yong-Hyun Kim [1,2,†]
[1]Department of Physics, Korea Advanced Institute of Science and Technology (KAIST), Daejeon 34141, Republic of Korea
[2]School of Physics, Institute of Science, Suranaree University of Technology, Nakhon Ratchasima 30000, Thailand

(Received 21 November 2024; accepted 7 September 2025; published 22 September 2025)

Despite extensive study and the practical significance of friction-driven static electricity, a quantitative triboelectric charge transfer theory has yet to be established. Here, we elucidate the detailed dynamics of triboelectric charge transfer driven by interfacial thermoelectric bias, maintaining a steady state at the interface. We demonstrate that transferred triboelectric charge exists in a deltalike distribution at a steady state and is dictated by half of the difference between thermoelectrically induced surface charges. Moreover, we quantitatively discuss electrostatic adhesion and static discharge between the transferred charges, which we may experience every day, including the role of surface charge inhomogeneity. Our findings may have significant implications for applications ranging from static electricity phenomena to advanced energy harvesting devices.

DOI: 10.1103/x3x7-s32f

Introduction. Triboelectric charging occurs when two surfaces acquire electric charge through the energy dissipation process, such as contact or friction. This phenomenon has productive applications such as xerography [1] and energy harvesting devices [2], but also detrimental onset such as sparks in microelectronics [3,4] and particle agglomeration in industrial polymers [5] or pharmaceuticals [6]. Moreover, triboelectric charging plays a key role in the solvent-free self-assembly of particles, organizing particles into ordered arrays without liquid media [7–10]. Recently, it has been reported that triboelectric charging has an intimate influence on daily coffee flavor via granular agglomeration during the grinding of roasted beans [11].

Despite its ubiquity, many researchers have struggled to understand triboelectric charging for several centuries. Historically, triboelectricity has been characterized using a triboelectric series, which empirically indicates the positive and negative charges between two materials [12]. However, the triboelectric series simply gives the qualitative charging trend, not the amount of charge transfer. Furthermore, the triboelectric series exhibits a low reproducibility and fails to account for several phenomena such as same-material charging [13–15] and triboelectric cycles [16,17]. To address these limitations, researchers have proposed various theoretical frameworks, including explanations based on (effective) work function difference [18–27], strain-driven polarization [28–31], and ion/material transfer [32–39]. Several studies have highlighted the role of water in triboelectric charging [11,40–44]. Nevertheless, while these arguments mainly focus on the underlying driving mechanisms of tribocharging, a quantitative prediction of charge transfer remains elusive.

Quantitative charge transfer models of triboelectricity have been proposed continuously, but with limitations. One of the widely proposed charge transfer models is the condenser (or capacitor) model, which treats the difference of either the work function or the contact potential as a potential difference across a capacitor [45,46]. It cannot explain the variations of charge transfer induced by several factors, such as surface asperities and trap states. Thus, the model is usually modified by a correction with experimental parameters, but even the modified models provide limited explanations. Beyond the condenser model, additional models have been proposed, but they still rely on experimental fitting parameters [45,46]. Recently, a quantitative model of triboelectric charge transfer without empirical parameters based on flexoelectricity has been reported [47]. However, this model is still limited to the metal-semiconductor interface, making it difficult to generalize to tribocharging with insulators. Thus, a more comprehensive theory, explicitly addressing the magnitude of triboelectric charge transfer, is required.

Recently, Shin and co-workers proposed an exactly solvable triboelectric mechanism based on the interfacial thermoelectric effect, providing physical parameters to quantitatively explain the triboelectric series [48]. Note that Henry and Harper suggested that the thermoelectric effect may play a role in triboelectricity [22,49]. The newly revisited mechanism reveals that heat generated between two semi-infinite materials induces a charge redistribution via the thermoelectric effect under open circuit conditions. This thermally induced charge redistribution leads to a net charge accumulation at the surface. By quantitatively defining the triboelectric factor $\xi = S/\sqrt{\rho c k}$, where S is the Seebeck coefficient, ρ is density, c is specific heat, and k is thermal conductivity, Shin and co-workers successfully estimated triboelectric charging polarities and quantified the thermoelectrically induced surface charge density. This surface charge density also exhibited saturation behavior with quantitative

*These authors contributed equally to this work.
†Contact author: yong.hyun.kim@kaist.ac.kr

Published by the American Physical Society under the terms of the Creative Commons Attribution 4.0 International license. Further distribution of this work must maintain attribution to the author(s) and the published article's title, journal citation, and DOI.

resemblance to experimental observations [48,50,51]. Moreover, theoretical concepts such as temperature profile and triboelectric factor have been gradually adopted in the triboelectric community [11,52–57]. Recently, Matsukawa and co-workers investigated the decomposition of molybdenum dithiocarbamate in nanoparticles and the formation of a MoS_2-containing tribofilm upon contact and release with diamondlike carbon and nanoparticles and particularly explained triboemission properties based on the difference in the triboelectric factor of rutile (−0.154) and anatase (−0.102) TiO_2 nanoparticles [57]. Even if the triboelectric factor provides a quantitative guiding principle to estimate the charging polarity of materials, it has not settled the quantification of the charge transfer to establish thermal equilibrium across the interface between two materials.

Here, we present a theoretical quantification method of triboelectric charge transfer driven by the interfacial thermoelectric effect, which has not been completely solved in our preceding study. Based on the steady state at the interface, we could elucidate that thermoelectric-driven triboelectric charge transfer is determined by half of each thermally induced surface charge. The transferred charge exhibits saturation behavior over time and predictable behavior in the triboelectric series. In addition, we discuss static phenomena, such as adhesion and discharge, considering surface charge inhomogeneity after tribocharging. Integrating these insights, we develop a comprehensive theory of triboelectric charge transfer driven by the thermoelectric effect in this work.

Thermoelectric-driven tribocharge transfer. Figure 1(a) shows the thermodynamic driving force from thermoelectricity; i.e., a voltage variation is generated within each material. Considering the complexity and diversity of friction at interfaces, we simplified these complex phenomena by representing them as frictional heat. Microscopically, friction between two semi-infinite materials occurs when an external force causes surface atoms to cross energy barriers in the weakly interacting regime, which can be regarded as the breaking of van der Waals bonds. Then, frictional heat is generated via a bond-breaking process corresponding to stationary heat pulses $\dot{Q}(x,t) = Q_0\delta(x)\sum_n^N \delta(t-n\tau)$ at the interface, where Q_0 denotes the energy of the frictional heat produced per pulse and τ is the interval between pulses. Estimating the van der Waals energy dissipation in a typical sliding speed of 10 cm/s, we set Q_0 as $0.01\,\mathrm{J/m^2}$ per $\tau = 1$ ns with a friction coefficient of $\mu = 0.1$ [48]. Since the use of a half-and-half heat partition does not change the underlying physics and is insensitive to interfacial thermal conductance, the temperature profile from the one-dimensional heat equation is analytically derived as follows:

$$T(x,t) = \frac{1}{2}\frac{Q_0/\tau}{\sqrt{\pi\rho ck}}\sqrt{t}\,\mathcal{E}_{3/2}\left[\frac{x^2}{4\alpha t}\right] \quad (\text{as } t \gg \tau), \qquad (1)$$

where $\mathcal{E}_m(z) = \int_1^\infty e^{-zu}/u^m\,du$ is the exponential integral function and α is the thermal diffusivity. The thermoelectric response is represented by $J = \sigma(E - S\nabla T)$, where J is the current density, σ is the electrical conductivity, E is the E-field, and T is the temperature distribution [48,58]. Considering that the dynamics of electrons is in femtoseconds [59], an instantaneous electronic equilibrium or open-circuit condition ($J = 0$) provides the potential $V = -ST$ and the charge distribution $\rho_0 = \varepsilon S\nabla^2 T$, where ε is the dielectric constant. The potential difference ΔV at the interface $x = 0$ of two contacting materials is

$$\Delta V = V_\mathrm{L} - V_\mathrm{R} = S_\mathrm{R}T_\mathrm{R}(0,t) - S_\mathrm{L}T_\mathrm{L}(0,t)$$
$$= \frac{Q_0}{\tau}\sqrt{t/\pi}\left[\frac{S_\mathrm{R}}{\sqrt{\rho_\mathrm{R}c_\mathrm{R}k_\mathrm{R}}} - \frac{S_\mathrm{L}}{\sqrt{\rho_\mathrm{L}c_\mathrm{L}k_\mathrm{L}}}\right], \qquad (2)$$

where subscripts L and R correspond to $x < 0$ and $x > 0$. This potential gap at the interface acts as a quantitative indicator of triboelectric hierarchy or polarity via the triboelectric factor ξ [48]. Currently, the material properties within this factor have used bulk properties as the first-order approximation to establish triboelectric series or polarity, but a more precise description of the thermoelectric-driven triboelectricity theory at the interface could be achieved if material properties that accurately capture interfacial variations were used. The interfacial thermoelectric response generates a thermally accumulated surface charge $\sigma_\mathrm{surface} = -\varepsilon SQ_0/(2k\tau)$ for the input heat Q_0. The σ_surface should be transferred due to the interfacial voltage bias, which has not been quantitatively discussed because of the open-circuit condition at the junction in our previous theory.

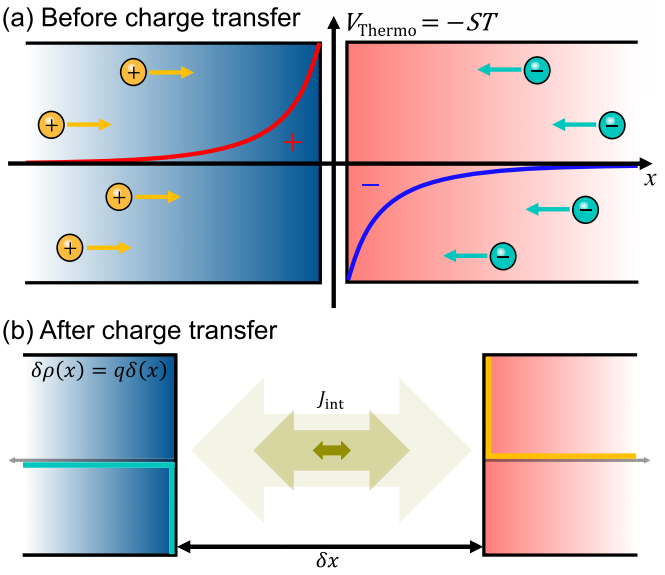


FIG. 1. Schematics of triboelectric charge transfer driven by thermoelectricity. (a) Voltage profile and charge accumulation caused by the thermoelectric effect under the open-circuit condition. Charge carriers are redistributed due to the temperature gradient and develop a substantial voltage difference at the interface. (b) Steady state of triboelectric charging after allowing charge transfer (J_int) or shorting the circuit. The voltage difference in an infinitesimal gap δx allows carriers to be transferred. Like the highly localized nature of charge diffusion in triboelectric systems, the transferred charge is represented by a Dirac delta distribution. Once triboelectric charge transfer is completed, a steady state at the interface is reached.

Figure 1(b) represents that the transferred triboelectric charge q has the distribution of a deltalike function, $\delta\rho(x) = q\delta(x)$, once a steady state at the interface is reached after allowing the charge transfer or shorting the circuit. A highly localized charge distribution on the surface is

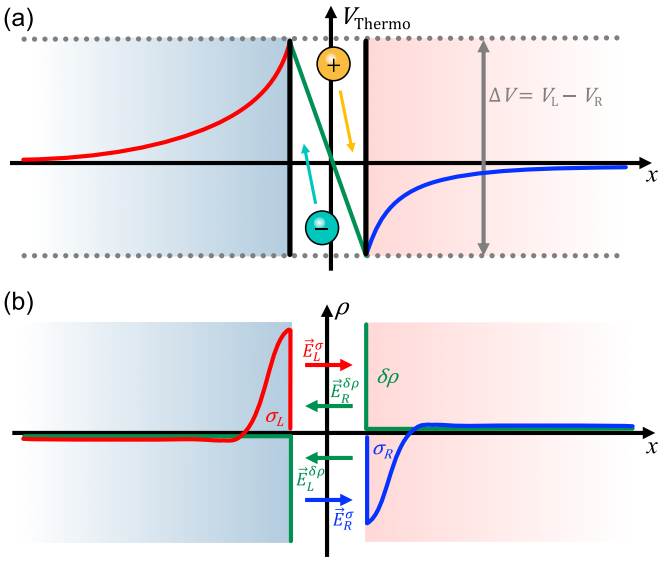


FIG. 2. Schematics of the charging mechanism at the interface. (a) The interfacial voltage gap induced by thermally induced surface charge. Charges accumulated by the thermoelectric voltage profile induce an interfacial voltage gap ΔV and thus can be transferred between two surfaces. (b) The interfacial E-field generated by the thermally induced surface charge and the transferred charge. The surface charges σ_{L} and σ_{R}, which are driven by the thermoelectric voltage profile, generate E-fields of $\vec{E}_{\text{L}}^{\sigma}$ and $\vec{E}_{\text{R}}^{\sigma}$, respectively. The transferred charge distribution $\delta\rho$ gives $\vec{E}_{\text{L}}^{\delta\rho}$ and $\vec{E}_{\text{R}}^{\delta\rho}$. For the steady state at the interface, the total E-field should be zero.

frequently observed in triboelectric systems [60–62]. Since the bulk thermoelectric response is already satisfied as $E = S\nabla T$, the transferred charge concentrates at the surface, forming the deltalike distribution. Moreover, this charge distribution is unique, as any deviation tends to decay over time (see Supplementary Note 1 of the Supplemental Material for details [63]). Based on this localized charge distribution, we could investigate the dynamics of the transferred charge by analyzing the interfacial electric field.

In Fig. 2(a), the thermoelectric potential difference ΔV enables charge transfer in the direction of interfacial voltage offset. A reverse bias formed by the transferred charge q in the unit of $\mu\text{C/m}^2$ leads to a steady state at the interface. Charge transfer occurs until the transferred charges compensate thermoelectric-induced charges corresponding to ΔV. Figure 2(b) illustrates the interfacial E-field generated by thermally induced surface charges ($\sigma_{\text{L,R}}$) and the transferred charges ($\delta\rho$). For the δ-type charge distribution, the transferred charges induce the E-field in the infinitesimal gap only. Thus, the interfacial E-field $\vec{E}_{\text{int}}$ is formulated as follows:

$$\vec{E}_{\text{int}} = \vec{E}_{\text{L}}^{\delta\rho} + \vec{E}_{\text{R}}^{\delta\rho} + \vec{E}_{\text{L}}^{\sigma} + \vec{E}_{\text{R}}^{\sigma} \tag{3a}$$

$$= -\frac{q}{\varepsilon_0} + \left(-\frac{\varepsilon_{\text{r,L}}}{2}\frac{S_{\text{L}}}{k_{\text{L}}} + \frac{\varepsilon_{\text{r,R}}}{2}\frac{S_{\text{R}}}{k_{\text{R}}}\right)\frac{Q_0}{2\tau}, \tag{3b}$$

where ε_0 and ε_{r} are the vacuum and relative permittivity, respectively. The first two terms $\vec{E}_{\text{L,R}}^{\delta\rho}$ in Eq. (3a) represent the E-field induced by the transferred charges, which is the same as the E-field between two infinite plates. The last two terms are the E-field caused by the thermally induced surface charges. Since $\vec{E}_{\text{int}}$ is zero once the steady state at the interface is reached, the transferred charge q in Eq. (3b) is as follows:

$$q = \left(-\frac{\varepsilon_{\text{L}}}{2}\frac{S_{\text{L}}}{k_{\text{L}}} + \frac{\varepsilon_{\text{R}}}{2}\frac{S_{\text{R}}}{k_{\text{R}}}\right)\frac{Q_0}{2\tau} = \frac{\sigma_{\text{L}} - \sigma_{\text{R}}}{2}, \tag{4}$$

where $\varepsilon_{\text{L,R}}$ and $\sigma_{\text{L,R}}$ are dielectric constants and the thermally accumulated surface charges of the left and right materials, respectively. Equation (4) shows that the transferred charge q is governed by half of the difference between the thermally induced surface charge densities in each material. In Eq. (1), the temperature profile generated by the frictional heat follows the function of $\mathcal{E}_{3/2}[x^2/4\alpha t]$. As time goes to infinity, the temperature profile near the interface can be approximated linearly as $T(x,t) \approx \frac{Q_0/\tau}{\sqrt{\pi\rho ck}}\sqrt{t} - \frac{Q_0/\tau}{2k}x$, corresponding to estimating the charge distribution at a steady-state temperature [64]. In this linear approximation, the thermoelectric response for charge carriers takes the form of the deltalike function at the surface. Consequently, after sufficient time passes, thermally accumulated surface charges directly influence the amount of the transferred charge.

Figure 3 shows the charging dynamics as a function of time and triboelectric pairs when subjected to frictional heat. To calculate the transferred charge q between triboelectric pairs, we obtain thermally induced surface charges for the triboelectric pairs using theoretical Seebeck coefficients, experimental thermal conductivities [48], and the experimental dielectric constants [65–76]. The theoretical Seebeck coefficient was estimated by comparing the charge neutrality energy from electronic structures to the hydrogen redox potential of −4.44 eV, which represents the probable Fermi level for materials in inevitable moisture [48,77].

Figure 3(a) shows the charging behavior of the PTFE-nylon pair, which is the most reproducible combination in the experiment. The transferred charge q presents the saturation behavior with a time constant τ_{t} estimated to be roughly 10 μs (see Supplementary Note 2 of the Supplemental Material for details [63]). This implies that triboelectric charging occurs in very short bursts. Because the PTFE and nylon have negative and positive Seebeck coefficients: $S_{\text{PTFE}} = -12.3\,\text{mV/K}$ and $S_{\text{nylon}} = +11.1\,\text{mV/K}$, each PTFE and nylon develops positive and negative σ_{surface}, respectively. Following Eq. (S3) of the Supplemental Material [63], each path in Fig. 3(a) means the charge transfer between a certain σ_{surface} and a neutral one (or superconductor). For example, the σ_{surface} of PTFE with a positive sign accepts an electron from a counterpart neutral material. The nylon donates electrons to the counterpart system. The σ_{surface} values of PTFE and nylon are calculated to be +4.4 and $-6.0\,\mu\text{C/m}^2$, which leads to $q = 5.2\,\mu\text{C/m}^2$ in Fig. 3(a). Notably, the theoretical estimation is quantitatively comparable to the experimental values of $\sim 3\,\mu\text{C/m}^2$ [51].

Finally, we calculated the transferred charges of y-axis materials rubbed against x-axis materials in the triboelectric series using Eq. (4), as shown in Fig. 3(b). The order of the triboelectric series comes from the previous study, with a remarkable similarity between the theoretical and experimental triboelectric series [48]. The more triboelectric pairs are separated, the more charge is usually transferred, which can be up to about $25\,\mu\text{C/m}^2$ for wool-PVC. Several pairs, such as nylon-silk, PE-sulfur, and PTFE-sulfur, show reverse polarity

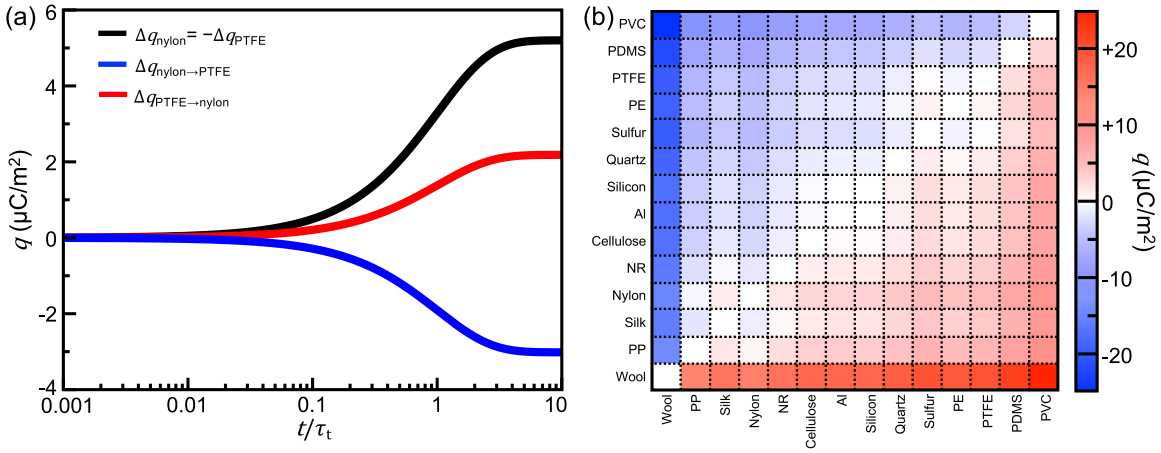


FIG. 3. Charging dynamics as a function of time and triboelectric pairs. (a) Charging dynamics of PTFE-nylon. τ_t is a time constant defined by $\tau_t^{-1} = \sigma_{int}/\varepsilon_0$, where σ_{int} is the interfacial electrical conductivity. The black line represents the net transferred charge between the PTFE-nylon pair. The nylon and PTFE are positively and negatively charged, respectively. The blue and red lines are charge transfers from nylon to PTFE and vice versa. (b) Comparison of charging between materials in the triboelectric series. All values correspond to the transferred charges of the y-axis materials rubbed against the x-axis materials. The red and blue colors are positively and negatively charged, respectively.

in the triboelectric series because nylon, PE, and PTFE exhibit larger $\sigma_{surface}$ values than silk and sulfur. For the nylon-silk pair, it has been reported that nylon is positively charged and silk is negatively charged [78,79]. For PE-sulfur and PTFE-sulfur pairs, the dielectric constant of solid sulfur is used to be 3.69 [74]. However, it can range from 1.5 to 1.8 in a compendium [80], which can change the sign and amount of the transferred charge. Moreover, the charging behavior of PTFE-Al and nylon-Al, i.e., insulator-metal, is solely determined by the $\sigma_{surface}$ of insulators. $S_{Al} = -2.5\,\mu V/K$ is almost negligible, which leads to an insignificant magnitude of $\sigma_{surface,Al}$. As a result, Eq. (4) is approximated to $q = \sigma_{surface,ins}/2$. Additionally, the quantification of charge transfer is indirectly applicable to the measurement of the Seebeck coefficient of insulators via the formula $\sigma_{surface} = -\varepsilon S Q_0/(2k\tau)$, which may be considered the most challenging issue in thermoelectric research.

Discussion. After triboelectric charging, electrostatic phenomena such as adhesion and discharge typically arise from the transferred triboelectric charges. To investigate these phenomena in detail, we examine how triboelectric charges influence the magnitude of electrostatic forces and the conditions for discharge. Although our model has considered that triboelectric surface charge is formed uniformly on flat surfaces, real material surfaces often exhibit an uneven distribution of charge due to surface morphology [81–83]. Since precisely analyzing realistic scenarios involving complex surface morphologies is challenging, we introduce a simple model with highly localized triboelectric surface charges, as shown in Fig. 4(a). Specifically, we assume that the charge is confined to the single and 2×2 patterns within a circular region of radius R on a contact area $A = 1\,cm^2$. The transferred charge q on this area gives a total charge $Q = qA$, where the 2×2 charges have a charge of $Q/4$ per circle. We set a separation distance between circular charges as 5 mm in the 2×2 charges, where all circular charges are equally located within the plane. By examining these cases of localized charge, we can identify the impact of charge inhomogeneity on electrostatic forces and discharge conditions, varying the gap distance d and the radius R.

Figure 4(b) compares the electrostatic forces due to the transferred charges between the uniform charge and circular charges. In the uniform charge, the electrostatic force $F = q^2A/2\varepsilon_0$ for PTFE-nylon is about 0.15 mN with $q = 5.2\,\mu C/m^2$, which can lift light objects weighing 15 mg. On the other hand, using Eq. (S4) of the Supplemental Material [63], the electrostatic force of the single and 2×2 charges can be larger than that for the uniform charge (see Supplementary Note 3 of the Supplemental Material for calculation details [63]). When the radius of localized charges decreases, the force can increase. In particular, the force at the specific distance has a local maximum. This implies that a stronger force is applied to prevent the charged materials from separating each other. Furthermore, since the thermally induced surface charge is proportional to the input heat Q_0, the thermoelectric-driven charge transfer could produce an enormous force if additional heat sources like Joule heating or photothermal heating are considered. Then, this force can be switched and its magnitude adjusted depending on the heat injection, enabling to apply electroadhesion to move or secure objects.

We also analyze the maximum potential difference ΔV generated by the localized charges with the breakdown voltage from Paschen's law, which is an empirical relation that defines the breakdown voltage necessary to initiate a discharge in various gases. Since triboelectric charging is typically generated in the air, we adopt Paschen's law of air [84]. Also, we use 1 atm of pressure by assuming slow separation of materials. As the small gap distance d between two materials fails to predict the breakdown voltage [85], we select $d = 0.1$ mm where Paschen's law is valid [86]. In Fig. 4(c), the potential difference of the uniform charge for the PTFE-nylon pair, $\Delta V_{uniform} = qd/\varepsilon_0$, does not reach the breakdown voltage of air, which means that triboelectric discharge cannot occur. On the other hand, the electric potential of the single and 2×2 charges with a radius smaller than a certain radius becomes

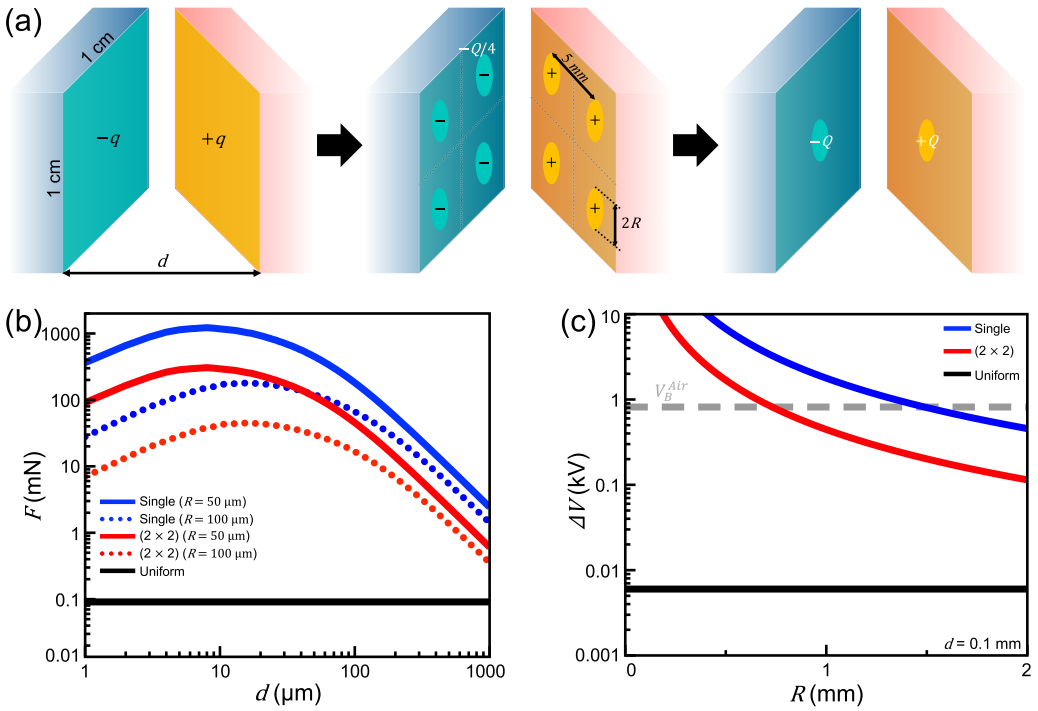


FIG. 4. Electrostatic force and discharge after triboelectric charging. (a) Schematic representation of surface charge localization. To test the inhomogeneity of the triboelectric surface charge, we evaluate the electrostatic force and discharge on two cases of localized triboelectric charges: a single and a 2 × 2 pattern of circular charges. A uniform surface charge density q, which is equal to the transferred charge, on an area $A = 1\,\mathrm{cm}^2$ gives a total charge $Q = qA$. Each of the four circles in the 2 × 2 pattern therefore carries $Q/4$. (b) Electrostatic force F exerted by triboelectric charges for the PTFE-nylon pair. The black line represents the force of the uniform charge. The blue and red lines show the force of the single and 2 × 2 charges, respectively. The solid and dotted lines correspond to circular-charge radii of 50 and 100 μm, respectively. (c) Potential difference ΔV produced by triboelectric charges for the PTFE-nylon pair. The blue, red, and black solid lines show the potential difference of the single, 2 × 2, and uniform charges, respectively. The gray dashed line marks the breakdown voltage of air given by Paschen's law. The gap distance between the two materials is 0.1 mm.

larger than the breakdown voltage (see Supplementary Note 3 of the Supplemental Material for calculation details [63]). This implies that localized charges can be one of the factors leading to triboelectric discharge.

Our theory addresses triboelectric charging between semi-finite materials driven by interfacial thermoelectric effects. According to our analysis, no driving force for triboelectric charging exists between identical materials. However, we predict that triboelectric charging between identical materials is primarily governed by higher-order interfacial effects such as material size, surface roughness, and curvature. When these effects are considered, even identical materials may exhibit different interfacial temperature profiles, thus enabling tribocharging. Indeed, it has been reported that triboelectric charging is enhanced on bumpy surfaces [87–89] and even occurs between identical materials [90–92]. To explain this, there is ongoing research into how much the charge or electrical interaction changes with surface roughness, but it is not yet well understood [93–95]. Future work will delve into these higher-order interfacial effects and their impacts on frictional heat generation and charge-transfer behavior. A rigorous understanding of these higher-order effects would be expected to explain charge mosaics, where positive and negative charges alternately coexist on a single contact surface [81,96–98].

As we mentioned in the introduction, water affects tribocharging in several ways [11,40–44]. Thus, the influence of humidity requires systematic exploration. In our model, we consider humidity to play a role in establishing a global Fermi level, thereby influencing the theoretical Seebeck coefficient [48,77]. However, water may also serve as a lubricant to reduce energy dissipation or affect heat transfer through absorption and evaporation. Moreover, water can also function as the number of defects, changing the chemical potential or affecting the surface morphology. A rigorous study of how water influences heat generation and charge transfer, as well as the ultimate role it plays in thermoelectric-driven tribocharging, is thus indispensable.

By analyzing how higher-order interfacial effects influence thermoelectric-driven triboelectric charging dynamics, we seek to develop a predictive framework for optimizing energy harvesting in triboelectric nanogenerators through engineered micro/nanostructured surfaces and tunable thermal gradients. This enables self-regulating triboelectric nanogenerators with adaptive power output under varying conditions. Beyond energy harvesting, controlled charge modulation has potential applications in electroadhesion for robotics, precision particle assembly in additive manufacturing, and electrostatic haptic interfaces.

Conclusion. In conclusion, thermoelectric-driven charge transfer offers a new way of achieving controllable triboelectric charge. We have confirmed that the steady-state condition at the interface induces the balance between

the thermodynamic driving force by the thermoelectric response in bulk charge carriers and the *E*-field from the transferred charge. The triboelectric factor is a more fundamental figure of merit to determine absolute charging polarity, but the thermally induced surface charge is a good indicator for the resultant transferred charge. By systematically tuning variables such as density, specific heat, thermal conductivity, and thermopower, our findings can be leveraged to optimize triboelectric nanogenerators and enhance their output, demonstrating the practical applicability of our approach in energy harvesting. Nevertheless, our model currently has limitations, particularly in explaining triboelectric charging between identical materials and fully addressing environmental factors such as humidity and temperature variations. Future research should systematically explore these aspects to enhance the robustness and applicability of the theory. Finally, we propose that the validation of thermoelectric-driven charge transfer could be realized via the control of thermally induced surface charge using systematically controllable thermoelectric materials such as metal-organic frameworks and carbon nanotube sheets, or via zero charging between superconductors with zero Seebeck coefficient [12].

Acknowledgment. This work was supported by the Grand Challenge 30 program from the College of Natural Sciences, KAIST.

[1] C. B. Duke, J. Noolandi, and T. Thieret, The surface science of xerography, Surf. Sci. **500**, 1005 (2002).
[2] F.-R. Fan, Z.-Q. Tian, and Z. L. Wang, Flexible triboelectric generator, Nano Energy **1**, 328 (2012).
[3] N. Gibson, Static electricity—An industrial hazard under control? J. Electrostat. **40–41**, 21 (1997).
[4] H. T. Baytekin, B. Baytekin, T. M. Hermans, B. Kowalczyk, and B. A. Grzybowski, Control of surface charges by radicals as a principle of antistatic polymers protecting electronic circuitry, Science **341**, 1368 (2013).
[5] G. Hendrickson, Electrostatics and gas phase fluidized bed polymerization reactor wall sheeting, Chem. Eng. Sci. **61**, 1041 (2006).
[6] K. C. Pingali, S. V. Hammond, F. J. Muzzio, and T. Shinbrot, Use of a static eliminator to improve powder flow, Int. J. Pharm. **369**, 2 (2009).
[7] B. A. Grzybowski, A. Winkleman, J. A. Wiles, Y. Brumer, and G. M. Whitesides, Electrostatic self-assembly of macroscopic crystals using contact electrification, Nat. Mater. **2**, 241 (2003).
[8] K. Sotthewes, G. Roozendaal, A. Šutka, and I. S. M. Jimidar, Toward the assembly of 2D tunable crystal patterns of spherical colloids on a wafer-scale, ACS Appl. Mater. Interfaces **16**, 12007 (2024).
[9] K. Sotthewes and I. S. M. Jimidar, Navigating the landscape of dry assembling ordered particle structures: Can solvents become obsolete? Small **20**, 2405410 (2024).
[10] S. Battat, D. A. Weitz, and G. M. Whitesides, Melting of a macroscale binary Coulombic crystal, Soft Matter **19**, 3190 (2023).
[11] J. M. Harper, C. S. McDonald, E. J. Rheingold, L. C. Wehn, R. E. Bumbaugh, E. J. Cope, L. E. Lindberg, J. Pham, Y.-H. Kim, J. Dufek, and C. H. Hendon, Moisture-controlled triboelectrification during coffee grinding, Matter **7**, 266 (2024).
[12] E.-C. Shin, J.-H. Mun, S. Baek, J. Jung, and Y.-H. Kim, Recent progress in understanding the microscopic origin of triboelectricity from mechanochemistry to thermoelectricity, Chem. Phys. Rev. **4**, 031305 (2023).
[13] P. E. Shaw, Electrical separation between identical solid surfaces, Proc. Phys. Soc. **39**, 449 (1926).
[14] D. J. Lacks and T. Shinbrot, Long-standing and unresolved issues in triboelectric charging, Nat. Rev. Chem. **3**, 465 (2019).
[15] K. Sotthewes, H. J. G. E. Gardeniers, G. Desmet, and I. S. M. Jimidar, Triboelectric charging of particles, an ongoing matter: From the early onset of planet formation to assembling crystals, ACS Omega **7**, 41828 (2022).
[16] P. E. Shaw and C. S. Jex, Tribo-electricity and friction. III.—Solid elements and textiles, Proc. R. Soc. London A **118**, 108 (1928).
[17] J. C. Sobarzo and S. Waitukaitis, Multiple charge carrier species as a possible cause for triboelectric cycles, Phys. Rev. E **109**, L032108 (2024).
[18] W. R. Harper, The Volta effect as a cause of static electrification, Proc. R. Soc. London A **205**, 83 (1951).
[19] F. A. Vick, Theory of contact electrification, Br. J. Appl. Phys. **4**, S1 (1953).
[20] A. R. Akande and J. Lowell, Charge transfer in metal/polymer contacts, J. Phys. D Appl. Phys. **20**, 565 (1987).
[21] W. R. Harper, *Contact and Frictional Electrification* (Laplacian Press, Morgan Hill, CA, 1998).
[22] W. R. Harper, Electrification following the contact of solids, Contemp. Phys. **2**, 345 (1961).
[23] Y. S. Zhou, S. Wang, Y. Yang, G. Zhu, S. Niu, Z.-H. Lin, Y. Liu, and Z. L. Wang, Manipulating nanoscale contact electrification by an applied electric field, Nano Lett. **14**, 1567 (2014).
[24] M. Seol, S. Kim, Y. Cho, K.-E. Byun, H. Kim, J. Kim, S. K. Kim, S.-W. Kim, H.-J. Shin, and S. Park, Triboelectric series of 2D layered materials, Adv. Mater. **30**, 1801210 (2018).
[25] S. Lin, L. Xu, C. Xu, X. Chen, A. C. Wang, B. Zhang, P. Lin, Y. Yang, H. Zhao, and Z. L. Wang, Electron transfer in nanoscale contact electrification: Effect of temperature in the metal-dielectric case, Adv. Mater. **31**, 1808197 (2019).
[26] H. Ko, Y. Lim, S. Han, C. K. Jeong, and S. B. Cho, Triboelectrification: Backflow and stuck charges are key, ACS Energy Lett. **6**, 2792 (2021).
[27] Z. Zhao, Y. Dai, D. Liu, X. Li, L. Zhou, B. Zhang, J. Wang, and Z. L. Wang, Achieving high contact-electrification charge density on inorganic materials, Nano Energy **114**, 108616 (2023).
[28] J. W. Peterson, The influence of piezo-electrification on triboelectrification, Phys. Rev. **76**, 1882 (1949).
[29] W. R. Harper, Adhesion and charging of quartz surfaces, Proc. R. Soc. London A **231**, 388 (1955).
[30] C. A. Mizzi, A. Y. W. Lin, and L. D. Marks, Does flexoelectricity drive triboelectricity? Phys. Rev. Lett. **123**, 116103 (2019).
[31] C. A. Mizzi and L. D. Marks, When flexoelectricity drives triboelectricity, Nano Lett. **22**, 3939 (2022).

[32] A. F. Diaz and D. Fenzel-Alexander, An ion transfer model for contact charging, Langmuir **9**, 1009 (1993).

[33] L. S. McCarty and G. M. Whitesides, Electrostatic charging due to separation of ions at interfaces: Contact electrification of ionic electrets, Angew. Chem. Int. Ed. **47**, 2188 (2008).

[34] H. Zhang, S. Sundaresan, and M. A. Webb, Thermodynamic driving forces in contact electrification between polymeric materials, Nat. Commun. **15**, 2616 (2024).

[35] Y. Fang, C. K. Ao, Y. Jiang, Y. Sun, L. Chen, and S. Soh, Static charge is an ionic molecular fragment, Nat. Commun. **15**, 1986 (2024).

[36] H. T. Baytekin, B. Baytekin, J. T. Incorvati, and B. A. Grzybowski, Material transfer and polarity reversal in contact charging, Angew. Chem. Int. Ed. **51**, 4843 (2012).

[37] A. E. Wang, P. S. Gil, M. Holonga, Z. Yavuz, H. T. Baytekin, R. M. Sankaran, and D. J. Lacks, Dependence of triboelectric charging behavior on material microstructure, Phys. Rev. Mater. **1**, 035605 (2017).

[38] P. C. Sherrell, A. Sutka, N. A. Shepelin, L. Lapcinskis, O. Verners, L. Germane, M. Timusk, R. A. Fenati, K. Malnieks, and A. V. Ellis, Probing contact electrification: A cohesively sticky problem, ACS Appl. Mater. Interfaces **13**, 44935 (2021).

[39] R. K. Pandey, H. Kakehashi, H. Nakanishi, and S. Soh, Correlating material transfer and charge transfer in contact electrification, J. Phys. Chem. C **122**, 16154 (2018).

[40] F. Galembeck, T. A. L. Burgo, L. B. S. Balestrin, R. F. Gouveia, C. A. Silva, and A. Galembeck, Friction, tribochemistry and triboelectricity: Recent progress and perspectives, RSC Adv. **4**, 64280 (2014).

[41] J. Nauruzbayeva, Z. Sun, A. Gallo Jr., M. Ibrahim, J. C. Santamarina, and H. Mishra, Electrification at water-hydrophobe interfaces, Nat. Commun. **11**, 5285 (2020).

[42] Y. Zhang, T. Pähtz, Y. Liu, X. Wang, R. Zhang, Y. Shen, R. Ji, and B. Cai, Electric field and humidity trigger contact electrification, Phys. Rev. X **5**, 011002 (2015).

[43] I. S. M. Jimidar, W. Kwiecinski, G. Roozendaal, E. S. Kooji, H. J. G. E. Gardeniers, G. Desmet, and K. Sotthewes, Influence of wettability and geometry on contact electrification between nonionic insulators, ACS Appl. Mater. Interfaces **15**, 42004 (2023).

[44] X. Bai, A. Riet, S. Xu, D. J. Lacks, and H. Wang, Experimental and simulation investigation of the nanoscale charge diffusion process on a dielectric surface: Effects of relative humidity, J. Phys. Chem. C **125**, 11677 (2021).

[45] S. Matsusaka, H. Maruyama, T. Matsuyama, and M. Ghadiri, Triboelectric charging of powders: A review, Chem. Eng. Sci. **65**, 5781 (2010).

[46] F. Chowdhury, M. Ray, A. Sowinski, P. Mehrani, and A. Passalacqua, A review on modeling approaches for the electrostatic charging of particles, Powder Technol. **389**, 104 (2021).

[47] K. P. Olson and L. D. Marks, A quantitative model of triboelectric charge transfer, Friction **13**, 9440937 (2025).

[48] E.-C. Shin, J.-H. Ko, H.-K. Lyeo, and Y.-H. Kim, Derivation of a governing rule in triboelectric charging and series from thermoelectricity, Phys. Rev. Res. **4**, 023131 (2022).

[49] P. S. H. Henry, The role of asymmetric rubbing in the generation of static electricity, J. Appl. Phys. **4**, S31 (1953).

[50] W. D. Greason, Investigation of a test methodology for triboelectrification, J. Electrostat. **49**, 245 (2000).

[51] G. Kleyman, T. Kang, J. Twiefel, and W. Voit, Characterization of triboelectric charge generation between PTFE and nylon after repeated contacts, Energy Harvest. Syst. **4**, 165 (2018).

[52] A. Sutka, K. Malnieks, M. Zubkins, A. Pludons, A. Sarakovskis, O. Verners, R. Eglitis, and P. C. Sherrell, Tribovoltaic performance of TiO_2 thin films: crystallinity, contact metal, and thermoelectric effects, ACS Appl. Mater. Interfaces **15**, 33140 (2023).

[53] Y. D. Ivanov, I. D. Shumov, A. F. Kozlov, M. O. Ershova, A. A. Valueva, I. A. Ivanova, V. Y. Tatur, A. A. Lukyanitsa, N. D. Ivanova, and V. S. Ziborov, Glycerol flow through a shielded coil induces aggregation and activity enhancement of horseradish peroxidase, Appl. Sci. **13**, 7516 (2023).

[54] J. H. Kim, J. Jeong, D. S. Kong, H. Y. Yoon, H. Cho, J. H. Jung, and J. Y. Park, Direct observation of contact electrification effects at nanoscale using scanning probe microscopy, Adv. Mater. Interfaces **11**, 2300821 (2024).

[55] H. Shin and D. Y. Kim, Energy-efficient electronics with an air-friction-driven rotating gate transistor using tribotronics, iScience **27**, 109029 (2024).

[56] K. Zhao, Z. Gao, J. Zhang, J. Zhou, F. Zhan, L. Qiang, M.-J. Liu, R.-H. Cyu, and Y.-L. Chueh, Design of strong-performance, high-heat dissipation rate, and long-lifetime triboelectric nanogenerator based on robust hexagonal boron nitride (hBN) nanosheets/polyvinyl chloride (PVC) composite films for rotational energy harvesting, J. Power Sources **614**, 234997 (2024).

[57] D. Matsukawa, J.-H. Park, W.-Y. Lee, T. Tokoroyama, J.-I. Kim, R. Ichino, and N. Umehara, Tribocatalytic reaction enabled by TiO_2 nanoparticle for MoDTC-derived tribofilm formation at ta-C/Steel contact, Coatings **14**, 773 (2024).

[58] E.-S. Lee, S. Cho, H.-K. Lyeo, and Y.-H. Kim, Seebeck effect at the atomic scale, Phys. Rev. Lett. **112**, 136601 (2014).

[59] H. Kim, Y. H. Chang, W.-J. Jang, E.-S. Lee, Y.-H. Kim, and S.-J. Kahng, Probing single-molecule dissociations from a bimolecular complex NO–Co-porphyrin, ACS Nano **9**, 7722 (2015).

[60] W. J. Brennan, J. Lowell, M. C. O'Neill, and M. P. W. Wilson, Contact electrification: The charge penetration depth, J. Phys. D. Appl. Phys. **25**, 1513 (1992).

[61] M. W. Williams, Triboelectric charging of insulators—Evidence for electrons versus ions, IEEE Trans. Ind. Appl. **47**, 1093 (2011).

[62] Y. S. Zhou, Y. Liu, G. Zhu, Z.-H. Lin, C. Pan, Q. Jing, and Z. L. Wang, *In situ* quantitative study of nanoscale triboelectrification and patterning, Nano Lett. **13**, 2771 (2013).

[63] See Supplemental Material at http://link.aps.org/supplemental/10.1103/x3x7-s32f for the details of deltalike charge distribution, electrostatic force, and the potential difference.

[64] G. D. Mahan, The low-temperature Seebeck coefficient in insulators, J. Electron. Mater. **44**, 431 (2015).

[65] J. Errera and H. S. Sack, Dielectric properties of animal fibers, Ind. Eng. Chem. Res. **35**, 712 (1943).

[66] P. K. C. Pillai, G. K. Narula, and A. K. Tripathi, Dielectric properties of polypropylene/polycarbonate polyblends, Polym. J. **16**, 575 (1984).

[67] S. Zhu and R. Langley, Dual-band wearable textile antenna on an EBG substrate, IEEE Trans. Antennas Propag. **57**, 926 (2009).

[68] W.-C. Yang, *Handbook of Fluidization and Fluid-Particle Systems* (CRC Press, Boca Raton, USA, 2003).

[69] S. K. De and J. R. White, *Rubber Technologist's Handbook* (Smithers Rapra Publishing, Shrewsburry, UK, 2001).

[70] Q. Luo, H. Shen, G. Zhou, and X. Xu, A mini-review on the dielectric properties of cellulose and nanocellulose-based materials as electronic components, Carbohydr. Polym. **303**, 120449 (2023).

[71] W. Zhou, Q. Chen, X. Sui, L. Dong, and Z. Wang, Enhanced thermal conductivity and dielectric properties of Al/β-SiC_w/PVDF composites, Compos. A: Appl. Sci. Manuf. **71**, 184 (2015).

[72] W. C. Dunlap and R. L. Watters, Direct measurement of the dielectric constants of silicon and germanium, Phys. Rev. **92**, 1396 (1953).

[73] V. E. Bottom, Dielectric constants of quartz, J. Appl. Phys. **43**, 1493 (1972).

[74] K. F. Young and H. P. R. Frederikse, Compilation of the static dielectric constant of inorganic solids, J. Phys. Chem. Ref. Data **2**, 313 (1973).

[75] Q. Tan, P. Irwin, and Y. Cao, Advanced dielectrics for capacitors, IEEJ Trans. Fundam. Mater. **126**, 1153 (2006).

[76] D. Tantraviwat, M. Ngamyingyoud, W. Sripumkhai, P. Pattamang, G. Rujijanagul, and B. Inceesungvorn, Tuning the dielectric constant and surface engineering of a $BaTiO_3$/porous PDMS composite film for enhanced triboelectric nanogenerator output performance, ACS Omega **6**, 29765 (2021).

[77] C. G. Van de Walle and J. Neugebauer, Universal alignment of hydrogen levels in semiconductors, insulators and solutions, Nature (London) **423**, 626 (2003).

[78] G. T. Dangelmayer, *Fundamentals of Electrostatics* (ESD Program Management, Boston, MA, 1990).

[79] N. Jonassen, *Electrostatics* (Springer US, Boston, MA, 1998).

[80] Dielectric constant (DC value): Compendium, Brochure, Endress+Hauser (2022), https://portal.endress.com/dla/5000894/4733/000/04/CP01076F00EN0322.pdf.

[81] H. T. Baytekin, A. Z. Patashinski, M. Branicki, B. Baytekin, S. Soh, and B. A. Grzybowski, The mosaic of surface charge in contact electrification, Science **333**, 308 (2011).

[82] T. A. L. Burgo, T. R. D. Ducati, K. R. Francisco, K. J. Clinckspoor, F. Galembeck, and S. E. Galembeck, Triboelectricity: Macroscopic charge patterns formed by self-arraying ions on polymer surfaces, Langmuir **28**, 7407 (2012).

[83] A. M. Barnes and A. D. Dinsmore, Heterogeneity of surface potential in contact electrification under ambient conditions: A comparison of pre- and post-contact states, J. Electrostat. **81**, 76 (2016).

[84] D. Liu, L. Zhou, S. Cui, Y. Gao, S. Li, Z. Zhao, Z. Yi, H. Zou, Y. Fan, J. Wang, and Z. L. Wang, Standardized measurement of dielectric materials' intrinsic triboelectric charge density through the suppression of air breakdown, Nat. Commun. **13**, 6019 (2022).

[85] E. Hourdakis, B. J. Simonds, and N. M. Zimmerman, Submicron gap capacitor for measurement of breakdown voltage in air, Rev. Sci. Instrum. **77**, 034702 (2006).

[86] R. T. Leon, P. C. Sherrell, J. I. Michel, J. Bullock, J. D. Berry, and A. V. Ellis, Understanding and controlling electrostatic discharge in triboelectric nanogenerators, ChemSusChem **17**, e202400366 (2024).

[87] S.-J. Park, M.-L. Seol, S.-B. Jeon, D. Kim, D. Lee, and Y.-K. Choi, Surface engineering of triboelectric nanogenerator with an electrodeposited gold nanoflower structure, Sci. Rep. **5**, 13866 (2015).

[88] Y. Zou, J. Xu, K. Chen, and J. Chen, Advances in nanostructures for high-performance triboelectric nanogenerators, Adv. Mater. Technol. **6**, 2000916 (2021).

[89] Z. Zhou, H. Qin, P. Cui, J. Wang, J. Zhang, Y. Ge, H. Liu, C. Feng, Y. Meng, Z. Huang, K. Yang, and G. Cheng, Enhancing the output of liquid-solid triboelectric nanogenerators through surface roughness optimization, ACS Appl. Mater. Interfaces **16**, 4763 (2024).

[90] O. Verners, L. Lapčinskis, L. Ģermane, A. Kasikov, M. Timusk, K. Pudzs, A. V. Ellis, P. C. Sherrell, and A. Šutka, Smooth polymers charge negatively: Controlling contact electrification polarity in polymers, Nano Energy **104**, 107914 (2022).

[91] C. Xu, B. Zhang, A. C. Wang, H. Zou, G. Liu, W. Ding, C. Wu, M. Ma, P. Feng, Z. Lin, and Z. L. Wang, Contact-electrification between two identical materials: Curvature effect, ACS Nano **13**, 2034 (2019).

[92] J. C. Sobarzo, F. Pertl, D. M. Balazs, T. Costanzo, M. Sauer, A. Foelske, M. Ostermann, C. M. Pichler, Y. Wang, Y. Nagata, M. Bonn, and S. Waitukaitis, Spontaneous ordering of identical materials into triboelectric series, Nature (London) **638**, 664 (2025).

[93] M. Feshanjerdi and A. Malekan, Contact electrification between randomly rough surfaces with identical materials, J. Appl. Phys. **125**, 165302 (2019).

[94] J. Wen, H. He, C. Niu, M. Rong, Y. Huang, and Y. Wu, An improved equivalent capacitance model of the triboelectric nanogenerator incorporating its surface roughness, Nano Energy **96**, 107070 (2022).

[95] K. P. Olson and L. D. Marks, Asperity shape in flexoelectric/triboelectric contacts, Nano Energy **119**, 109036 (2024).

[96] M. Sakaguchi, M. Makino, T. Ohura, and T. Iwata, Contact electrification of polymers due to electron transfer among mechano anions, mechano cations and mechano radicals, J. Electrostat. **72**, 412 (2014).

[97] Y. I. Sobolev, W. Adamkiewicz, M. Siek, and B. A. Grzybowski, Charge mosaics on contact-electrified dielectrics result from polarity-inverting discharges, Nat. Phys. **18**, 1347 (2022).

[98] G. Grosjean and S. Waitukaitis, Asymmetries in triboelectric charging: Generalizing mosaic models to different-material samples and sliding contacts, Phys. Rev. Mater. **7**, 065601 (2023).